A generalized ratiometric chemical exchange saturation transfer (CEST) MRI approach for mapping renal pH using iopamidol

A Generalized Ratiometric Chemical Exchange Saturation Transfer (CEST) MRI Approach for Mapping Renal pH using Iopamidol

Journal:	*Magnetic Resonance in Medicine*
Manuscript ID	Draft
Wiley - Manuscript type:	Note
Date Submitted by the Author:	n/a
Complete List of Authors:	Wu, Yin; Paul C. Lauterbur Research Centre for Biomedical Imaging, Institute of Biomedical and Health Engineering, Shenzhen Institutes of Advanced Technology, Chinese Academy of Sciences; Key Laboratory of Health Informatics, Chinese Academy of Sciences Zhou, Iris; Massachusetts General Hospital, Martinos Center; Harvard Medical School, Igarashi, Takahiro; Massachusetts General Hospital, Martinos Center Longo, Dario; CNR, Institute of Biostructure and Bioimaging; Molecular Imaging Center, Molecular Biotechnology and Health Sciences Aime, Silvio; University of Turin, Chemistry IFM Sun, Phillip; Harvard Medical School, Radiology
Research Type:	Contrast agents < Contrast < Biophysics < Technical Research, Magnetization transfer < Technique Development < Technical Research
Research Focus:	Other tissues (body fluids, skin, vessels, arteries, other organs, etc)

A Generalized Ratiometric Chemical Exchange Saturation Transfer (CEST) MRI Approach for Mapping Renal pH using Iopamidol

Yin Wu,[1,2] Iris Y. Zhou,[1] Takahiro Igarashi,[1] Dario L. Longo,[3] Silvio Aime,[4] and Phillip Zhe Sun [1]*

[1] Athinoula A. Martinos Center for Biomedical Imaging, Department of Radiology, Massachusetts General Hospital and Harvard Medical School, Charlestown, MA 02129, USA

[2] Paul C. Lauterbur Research Centre for Biomedical Imaging, Shenzhen Key Laboratory for MRI, Shenzhen Institutes of Advanced Technology, Chinese Academy of Sciences, Shenzhen, Guangdong 518055, China

[3] Institute of Biostructure and Bioimaging (CNR) c/o Molecular Biotechnology Center, University of Torino, Torino, Italy

[4] Department of Molecular Biotechnology and Health Sciences, Molecular Imaging Center, University of Torino, Torino, Italy

Correspondence Author:

Phillip Zhe Sun, PhD (pzhesun@mgh.harvard.edu)

Athinoula A. Martinos Center for Biomedical Imaging

Massachusetts General Hospital and Harvard Medical School

Charlestown, MA 02129, USA

Phone: (1) 617-726-4060; Fax: (1) 617-726-7422

Word Counts: 2,375

Running title: Generalized Ratiometric CEST renal pH imaging

ABSTRACT

Purpose

To extend the pH detection range of iopamidol-based ratiometric chemical exchange saturation transfer (CEST) MRI at sub-high magnetic field and establish quantitative renal pH MRI.

Methods

CEST imaging was performed on iopamidol phantoms with pH of 5.5-8.0 and in vivo on rat kidneys (N = 5) during iopamidol administration at a 4.7 Tesla. Iopamidol CEST effects were described using a multi-pool Lorentzian model. A generalized ratiometric analysis was conducted by ratioing resolved iopamidol CEST effects at 4.3 and 5.5 ppm obtained under 1.0 and 2.0 μT, respectively. The pH detection range was established for both the conventional ratiometric analysis and the proposed approach. Renal pH was mapped in vivo with regional pH assessed by one-way ANOVA.

Results

Good fitting performance was observed in multi-pool Lorentzian decoupling of CEST effects, both in the iopamidol phantom and rat kidneys (R^2s > 0.99). The proposed approach extends the in vitro pH detection range to 5.5-7.5 at 4.7 Tesla. In vivo renal pH was measured to be 7.0±0.1, 6.8±0.1 and 6.5±0.2 for cortex, medulla and calyx, respectively ($P<0.05$).

Conclusion

The proposed ratiometric approach extended the iopamidol pH detection range, enabled renal pH mapping in vivo, promising for pH imaging studies at sub-high or low fields with potential clinical applicability.

Key words: Chemical exchange saturation transfer; ratiometric imaging, kidney, pH, iopamidol

INTRODUCTION

Magnetic resonance imaging (MRI) serves as a versatile technique to assess kidney functionality. As kidney plays a vital role in balancing body acid/base homeostaisis, pH MRI is promising to identify renal dysfunction, diagnose regional kidney injury before symptom onset and ultimately, guide treatment prior to irreversible damage (1-3). However, conventional pH measurement techniques, including lactate, phosphorous and hyperpolarized ^{13}C magnetic resonance spectroscopy (MRS) are limited for routine renal imaging due to their relatively coarse spatiotemporal resolution or requirement of polarization devices (4-8). Gadolinium-based pH imaging provides novel insight of renal physiology and its disruption, yet it requires independent determination of local contrast agent concentration (9,10). Although this can be achieved by administering a second pH-insensitive agent with identical tissue pharmacokinetics, the repeated injection of contrast agents makes it somewhat cumbersome (1,11). The development of pH-sensitive PET/MRI hybrid contrast agent elegantly harnesses the pH sensitivity, MRI resolution and PET quantification of contrast agent concentration for pH mapping. However, this approach requires simultaneous PET and MRI acquisition, which is not widely available yet (12).

Iopamidol, an FDA-approved computed tomography contrast agent, has two distinct MR visible chemical exchangeable groups of different pH-dependent exchange rate. The development of ratiometric chemical exchange saturation transfer (CEST) MRI enables concentration-independent pH imaging (13-15). Its pH detection range has been shown to be 5.5-7.4 at 7 Tesla (T) and 6.0-7.6 at 14 T (16,17). Additional CEST agents have been investigated for pH imaging, including iopromide (18), imidazoles (19), and paramagnetic CEST (paraCEST) agents (20). Recently, radio-frequency (RF) power-based ratiometric pH MRI has been proposed that enables ratiometric MRI using iobitridol, a CEST agent with a single exchangeable group, for renal pH imaging (21). It is worthwhile to point out that most renal pH MRI studies thus far have been demonstrated at high fields (≥ 7 Tesla). When translated to low/sub-high field, the dynamic pH range has been substantially reduced due to

overlapped CEST effects and more prominent concomitant saturation transfer effects (16,22). As renal pH spans a relatively broad range, (1,2,16,21), our study aimed to devise a new means of ratiometric CEST MRI to enable renal pH imaging at 4.7 T as a pertinent step forward toward clinical application.

METHODS

MRI studies

The prospective study was conducted on a 4.7 T small-bore MRI scanner (Bruker Biospec, Billerica, MA). We used iopamidol phosphate buffered solution (PBS) phantom for pH calibration (16). Briefly, pH of 40 mM iopamidol PBS solution was titrated to 5.5, 6.0, 6.5, 7.0, 7.5 and 8.0, and imaged under 37°C. We used single-shot spin-echo (SE) echo planar imaging (EPI) with a field of view (FOV) of 52×52 mm^2, image matrix = 96×96 and slice thickness = 5 mm. We collected two Z-spectra for RF power (B_1) levels of 1.0 and 2.0 μT (frequency offsets between ±7 ppm with intervals of 0.25 ppm, repetition time (TR)/saturation time (TS)/echo time (TE)=10,000/5,000/48 ms). Water saturation shift referencing (WASSR) map was collected with B_1=0.3 μT (frequency offsets between ±0.125 ppm with intervals of 0.025 ppm, TR/TS=2,000/1,000 ms).

In vivo experiments have been approved by the local Institutional Animal Care and Use Committee. Briefly, adult male Wistar rats (N = 5, 292± 28g) were initially anesthetized with 5% isoflurane. Endotracheal intubation was performed after the animal was sufficiently anesthetized. The animals were mechanically ventilated at a rate of 60±2 bpm with 1.5-2% isoflurane in room-temperature air using a ventilator (Kent Scientific, Torrington, CT). Their body temperature was maintained at 37°C by a circulating warm water jacket positioned around the torso. A single slice image along the long axis of kidney was imaged with CEST MRI during iopamidol administration (FOV= 20×20 mm^2, image matrix = 48×48, slice thickness = 4 mm). Briefly, iopamidol (Isovue200, 1.5 mg I/g b.w.) was infused at a typical clinical dose via the tail vein using a syringe pump, with bolus injection of half of the dose at a rate of 18 ml/hr and continuous infusion of the rest of the contrast agent at a rate of 2 ml/hr during the CEST image acquisition. Respiratory gating was implemented before RF

saturation and data acquisition. WASSR map (frequency offsets between ±0.5 ppm with intervals of 0.05 ppm, B_1=0.3 μT) and two Z-spectra (frequency offsets between ±7 ppm with intervals of 0.125 ppm, TR/TS/TE = 6,000/3,000/18 ms) with B_1 levels of 1.0 and 2.0 μT were collected (15). The total scan time was approximately 45 min.

Data analysis

Data were analyzed in MATLAB (MathWorks, Natick, MA). Z-spectra (M_Z) were centered using the WASSR map and normalized by the signal without RF irradiation (M_0) (23,24). The Z-spectra were inverted as ($1-M_z/M_0$) and decoupled using a multi-pool Lorentzian model,

$$Z(w) = \sum_{i=1}^{7} L_i(w) \qquad \text{Eq. (1)}$$

where L_i is the Lorentzian spectrum of the i^{th} pool. Saturation transfer effects, including nuclear overhauser effect (NOE), magnetization transfer (MT), direct water saturation, iopamidol CEST effects of two hydroxyl groups (-OH) and two amide groups were solved using multi-pool Lorentzian model, with their chemical shifts at -3.2, -1.5, 0, 0.8, 1.8, 4.3 and 5.5 ppm, respectively (25,26),

$$L(w) = \frac{A}{1 + 4(\frac{w - w_0}{lw})^2} \qquad \text{Eq. (2)}$$

where w is the frequency offset, A, w_0, and lw are the amplitude, center frequency and linewidth of the i^{th} saturation transfer effects, respectively.

To minimize the bias of initial guesses, a recently developed Image Downsampling Expedited Adaptive Least-squares (IDEAL) fitting method was used (27). Briefly, CEST images were down-sampled to a single pixel to achieve high signal-to-noise ratio (SNR) for the initial fitting. Relaxed constraints were chosen, with peak and linewidth bounds between 1% and 100 times of the initial guesses, and the peak frequency shift within ±0.2 ppm of each chemical shift. CEST images were then resampled to 2×2, 4×4, 8×8, 12×12, 24×24 till the original resolution of 48×48, with the initial guesses of each voxel determined from the fitting results of the nearest voxel from the last down-sampled images. The

constraints were reduced to between 10% and 10 times of the iterative initial values. Nonlinear constrained fitting algorithm was used with two-fold overweighting applied for Z-spectra between 4.0 and 5.8 ppm to increase the fitting accuracy of iopamidol CEST effects at 4.3 and 5.5 ppm. Goodness of fitting (R^2) was calculated for each pixel. Ratiometric measurement was obtained by ratioing multi-Lorentzian model decoupled ST effects at 5.5 ppm obtained under B_1 of 2.0 μT to that at 4.3 ppm obtained under B_1 of 1.0 μT,

$$R_{ST} = \frac{ST_{5.5\,ppm,2.0\mu T}}{ST_{4.3\,ppm,1.0uT}} \quad \text{Eq. (3)}$$

For the conventional ratiometric methods, the ST effects at chemical shifts of 4.3 and 5.5 ppm were measured with asymmetric analysis of $ST(\omega) = \frac{M(-\omega)-M(\omega)}{M_0}$, where ω is the chemical shift of iopamidol amide proton with respective to the water resonance. To calibrate ratiometric CEST effect toward absolute pH, in vitro pH calibration was obtained using a polynomial fitting of R_{ST} as a function of titrated pH (16). The standard deviation of precision (SDP) was calculated (18). Renal pH from ratiometric analysis of the same RF power level (e.g. ST(5.5 ppm)/ST(4.3 ppm) under 1.0 and 2.0 μT) and mixed RF power levels (e.g. ST(5.5 ppm, 2.0 μT)/ST(4.3 ppm, 1.0 μT) and ST(5.5 ppm, 1.0 μT)/ST(4.3 ppm, 2.0 μT)) was investigated for both of the proposed and conventional ratiometric methods (Supplementary Information). One-way analysis of variance (ANOVA) with Bonferroni correction was conducted and P values less than 0.05 were considered statistically significant.

RESULTS

Figure 1 shows two representative CEST Z-spectra from the iopamidol PBS phantom (pH=7.0) obtained under B_1 of 1.0 and 2.0 μT. There is substantial overlap between iopamidol CEST effects at 4.3 and 5.5 ppm, with 4.3 ppm signal much stronger than that of 5.5 ppm. Multi-pool Lorentzian line decoupling (Eq. 1) resolves multiple overlapping CEST effects from the Z-spectrum, allowing improved calculation of the ratiometric analysis. Note that high R^2s >0.99 were achieved for all vials and power levels, indicating good fitting performance.

Figure 2 shows that the ratiometric analysis of decoupled CEST effects extended the range of pH detection from that using the conventional ratiometric analysis. Specifically, the routine ratiometric analysis (blue squares) has a narrow pH range of 5.5-7.0. This is because for pH above 7.0, chemical exchange rate at 5.5 ppm becomes relatively fast with respect to that of 4.3 ppm, making it inefficient to detect using moderate RF saturation power levels. Note that the pH detection range determined in vitro (i.e. 5.5-7.0) will likely be reduced when translated in vivo due to more pronounced concomitant magnetization transfer and direct saturation effects in tissue. Fortunately, the modified ratiometric analysis of decoupled CEST effects extended the pH detection range to 5.5-7.5 (SDP = 0.12 pH unit), aiding in vivo renal pH imaging. Figure 3 shows in vitro CEST images from the conventional asymmetry analysis at 5.5 ppm (B_1=2.0 μT, Fig. 3a) and at 4.3 ppm (B_1=1.0 μT, Fig. 3b). The conventional ratiometric image (Fig. 3c) can map pH up to 7.0 (Fig. 3d). In comparison, Figs. 3e and 3f show CEST images obtained from the line-decoupling approach, with the modified ratiometric image shown in Fig. 3g. The modified ratiometric analysis is sensitive to pH as high as 7.5 (Fig. 3h), extending from the relatively narrow pH range obtainable using the conventional ratiometric analysis.

Figure 4 shows inverted Z-spectra (i.e., 1-M_z/M_0) from regions of calyx, medulla and cortex of a representative rat kidney following iopamidol injection, obtained under B_1 of 1.0 μT (left column) and 2.0 μT (right column), fitted with a multi-pool Lorentzian model. The amplitude of CEST effect at 5.5 ppm decreases from calyx to cortex under B_1 of 2.0 μT, whereas the ST effect at 4.3 ppm shows relatively small change under B_1 of 1.0 μT, suggesting consecutive renal pH decrease from the outermost to the innermost layers. Good fitting was observed for all layers with R^2>0.99. We further confirmed that the modified ratiometric pH imaging provides improved renal pH mapping in vivo. Figures 5 a-c show decoupled CEST effects at 5.5 ppm (2.0 μT), 4.3 ppm (1.0 μT) and the generalized ratiometric images, respectively. Good fitting was observed for majority of voxels with R^2>0.99 (not

shown). Figure 5d shows renal pH map overlaid on a T_2-weighted image. pH was found to be 7.0 ± 0.1, 6.8 ± 0.1 and 6.5 ± 0.2 for cortex, medulla and calyx, respectively, significantly different from each other ($P<0.05$). To demonstrate the advantage of the modified pH mapping, we investigated renal pH from ratiometric analysis of the same RF power level at 4.7 T (e.g. ST(5.5 ppm)/ST(4.3 ppm) under 1.0 and 2.0 μT) and ST(5.5 ppm, 1.0 μT)/ST(4.3 ppm, 2.0 μT)), all showing unsatisfactory results (Supplementary Data). For example, ratiometric analysis of ST(5.5 ppm)/ST(4.3 ppm) under 1.0 μT yielded underestimated renal pH of 6.4±0.2, 6.2±0.3 and 5.8±0.3 for cortex, medulla and calyx, respectively (Supplementary Table 1). This suggests that the presence of pronounced concomitant MT and direct saturation effects substantially confound in vivo pH determination using conventional ratiometric analysis at sub-high/low field.

DISCUSSION

Our study generalized the routine ratiometric CEST analysis by mixing both RF power level and chemical shift for the ratiometric analysis, further applied multi-pool Lorentzian model to resolve overlapped CEST effects, and extended the range of pH detection at sub-high magnetic field. The approach was applied to measure renal pH in vivo, providing pH quantification in good agreement with prior findings at high field (2,19).

It has been shown that chemical exchange rate of iopamidol amide groups at 4.3 and 5.5 ppm are both dominantly base-catalyzed, and the exchange rate at 5.5 ppm increases much more rapidly with pH than that at 4.3 ppm (26). In addition, it has been well recognized that it takes higher RF irradiation level to effectively saturate exchangeable groups undergoing faster chemical exchange. Therefore, we extended the ratiometric pH imaging by ratioing CEST effects at mixed RF power levels and offsets so that CEST effect at 5.5 ppm obtained under a higher RF power was normalized by CEST effect at 4.3 ppm using a slightly lower RF power level. This is in contrast to prior ratiometric analysis that ratios CEST effects at different chemical shifts obtained under the same saturation power or

compares CEST effects at the same chemical shift obtained under different saturation levels. The proposed approach decoupled confounding concomitant saturation effects, therefore, provides robust pH mapping. It helps to briefly discuss the selection of RF power levels for the modified ratiometric analysis. Previous study shows that the contrast to noise of in vitro iopamidol pH imaging using the conventional ratiometric pH analysis peaks for B_1 of 2.5 μT at 4.7 T (26). To account for more pronounced concomitant MT and spillover effects in vivo, we reduced the B_1 level to 2.0 μT. A second RF power level is needed for the generalized ratiometric pH analysis. We chose an intermediate RF power level of 1 μT to balance between sufficient CEST effects without excessive broadening.

Our study found that renal pH gradually decreases from cortex, medulla to calyx, similar to those obtained using pH-sensitive Gd-based contrast agent (1). The mean pH for the entire kidney was 6.9±0.1, comparable to that reported previously (2,19). By referencing the corresponding pH and decoupled saturation transfer effects at 4.3 and 5.5 ppm from the phantom, averaged iopamidol concentration estimated from the two saturation effects was 14.1±5.0, 16.9±3.5, and 20.9±7.1 mM in cortex, medulla and calyx, respectively. The normalized iopamidol concentration in cortex and medulla with respect to that in the calyx was 67±7% and 84±10%, respectively. The trend of normalized iopamidol concentration significantly increased from cortex, medulla to calyx, consistent with the known renal physiology.

It has been recognized that proper selection of initial guesses is critical for quantitative CEST fitting, particularly for cases with suboptimal SNR, relatively large range of pH, and heterogeneous contrast agent distribution. Our study here first increased SNR by down-sampling CEST-weighted images, and the enhanced SNR and relaxed constraints warrant good estimation of fitting coefficients. The fitting results determined under good SNR were used as initial guesses for the quantitative CEST analysis, enabling semiautomatic and adaptive fitting per pixel. Notably, this approach allows using a

single set of initial guesses for the multi-pool Lorentzian model and fits all pixels in the kidney. Indeed, good fitting performance was achieved for both phantom and in vivo kidney studies.

CONCLUSION

Our study generalized the conventional ratiometric CEST analysis, extended the iopamidol pH MRI detection range, and further demonstrated renal pH in vivo at sub-high magnetic field.

ACKNOWLEDGEMENTS

This study was supported in part by National Natural Science Foundation of China (81571668), National Basic Research Program of China (2015CB755500), Shenzhen Science and Technology Program (GJHZ20160229200622417) and National Institute of Health (R01NS083654).

Figure Captions

Figure 1. Multi-pool Lorentzian decoupling of representative CEST Z-spectra from pH vial of 7.0, obtained under B_1 of (a) 1.0 μT and (b) 2.0 μT.

Figure 2. Extension of pH detection range using the modified ratiometric analysis (red circles) vs. that using the conventional simplistic ratiometric approach (blue squares).

Figure 3. Simplistic CESTR images (a) at 5.5 ppm acquired at 2.0 μT and (b) at 4.3 ppm obtained under 1.0 μT. (c) Ratiometric images show good pH sensitivity until pH of 7.0 (d). In comparison, (e) and (f) show CEST images obtained from the line-decoupling, with the modified ratiometric image shown in (g) that can capture pH as high as 7.5 (h).

Figure 4. Inverted Z-spectra measured at calyx (a, b), medulla (c, d), and cortex (e, f) from B_1 of 1.0 μT (left column) and 2.0 μT (right column) were fitted using a multi-pool Lorentzian model. ST effects at 5.5 ppm (B_1=2.0 μT, right column) decreases substantially from calyx (b), medulla (d), to cortex (f), while ST effect at 4.3 ppm (B_1=1.0 μT, left column) shows relatively small change (a, c, e).

Figure 5. Demonstration of renal pH map from a representative rat. The resolved maps of ST effects at (a) 5.5 and (b) 4.3 ppm were obtained with the decoupling method, from which (c) the modified ratiometric map was obtained. (d) pH map overlaid on corresponding T_2-weighted image shows renal pH gradually decreases from the cortex, medulla to calyx.

References

1. Raghunand N, Howison C, Sherry AD, Zhang S, Gillies RJ. Renal and systemic pH imaging by contrast-enhanced MRI. Magn Reson Med 2003;49(2):249-257.

2. Longo DL, Busato A, Lanzardo S, Antico F, Aime S. Imaging the pH evolution of an acute kidney injury model by means of iopamidol, a MRI-CEST pH-responsive contrast agent. Magn Reson Med 2013;70(3):859-864.

3. Wang F, Kopylov D, Zu Z, Takahashi K, Wang S, Quarles CC, Gore JC, Harris RC, Takahashi T. Mapping murine diabetic kidney disease using chemical exchange saturation transfer MRI. Magnetic Resonance in Medicine 2016;76(5):1531-1541.

4. Stubbs M, Bhujwalla ZM, Tozer GM, Rodrigues LM, Maxwell RJ, Morgan R, Howe FA, Griffiths JR. An assessment of 31P MRS as a method of measuring pH in rat tumours. NMR Biomed 1992;5(6):351-359.

5. van Sluis R, Bhujwalla ZM, Raghunand N, Ballesteros P, Alvarez J, Cerdan S, Galons JP, Gillies RJ. In vivo imaging of extracellular pH using 1H MRSI. Magn Reson Med 1999;41(4):743-750.

6. Garcia-Martin ML, Herigault G, Remy C, Farion R, Ballesteros P, Coles JA, Cerdan S, Ziegler A. Mapping extracellular pH in rat brain gliomas in vivo by 1H magnetic resonance spectroscopic imaging: comparison with maps of metabolites. Cancer Res 2001;61(17):6524-6531.

7. Gallagher FA, Kettunen MI, Day SE, Hu DE, Ardenkjaer-Larsen JH, Zandt R, Jensen PR, Karlsson M, Golman K, Lerche MH, Brindle KM. Magnetic resonance imaging of pH in vivo using hyperpolarized 13C-labelled bicarbonate. Nature 2008;453(7197):940-943.

8. Alvarez-Pérez J, Ballesteros P, Cerdán S. Microscopic images of intraspheroidal pH by 1H magnetic resonance chemical shift imaging of pH sensitive indicators. Magnetic Resonance Materials in Physics, Biology and Medicine 2005;18(6):293-301.

9. Zhang S, Wu K, Sherry AD. A Novel pH-Sensitive MRI Contrast Agent. Angew Chem Int Ed Engl 1999;38(21):3192-3194.

10. Garcia-Martin ML, Martinez GV, Raghunand N, Sherry AD, Zhang S, Gillies RJ. High resolution pH(e) imaging of rat glioma using pH-dependent relaxivity. Magn Reson Med 2006;55(2):309-315.

11. Beauregard DA, Parker D, Brindle KM. Relaxation-based mapping of tumor pH. 1998; Sydney, Australia. In: Proceedings of the 6th Annual Meeting of ISMRM. p 53.

12. Frullano L, Catana C, Benner T, Sherry AD, Caravan P. Bimodal MR-PET agent for quantitative pH imaging. Angew Chem Int Ed Engl 2010;49(13):2382-2384.

13. Aime S, Calabi L, Biondi L, De Miranda M, Ghelli S, Paleari L, Rebaudengo C, Terreno E. Iopamidol: Exploring the potential use of a well-established x-ray contrast agent for MRI. Magn Reson Med 2005;53(4):830-834.

14. Ward KM, Balaban RS. Determination of pH using water protons and chemical exchange dependent saturation transfer (CEST). Magn Reson Med 2000;44(5):799-802.

15. Wu R, Longo DL, Aime S, Sun PZ. Quantitative description of radiofrequency (RF) power-based ratiometric chemical exchange saturation transfer (CEST) pH imaging. NMR Biomed 2015;28(5):555-565.

16. Longo DL, Dastru W, Digilio G, Keupp J, Langereis S, Lanzardo S, Prestigio S, Steinbach O, Terreno E, Uggeri F, Aime S. Iopamidol as a responsive MRI-chemical exchange saturation transfer contrast agent for pH mapping of kidneys: In vivo studies in mice at 7 T. Magn Reson Med 2011;65(1):202-211.

17. Sheth VR, Liu G, Li Y, Pagel MD. Improved pH measurements with a single PARACEST MRI contrast agent. Contrast Media Mol Imaging 2010;7(1):26-34.

18. Moon BF, Jones KM, Chen LQ, Liu P, Randtke EA, Howison CM, Pagel MD. A comparison of iopromide and iopamidol, two acidoCEST MRI contrast media that measure tumor extracellular pH. Contrast Media Mol Imaging 2015;10(6):446-455.

19. Yang X, Song X, Banerjee SR, Li Y, Byun Y, Liu G, Bhujwalla ZM, Pomper MG, McMahon MT. Developing imidazoles as CEST MRI pH sensors. Contrast media & molecular imaging 2016;11(4):304-312.

20. Wu Y, Zhang S, Soesbe TC, Yu J, Vinogradov E, Lenkinski RE, Sherry AD. pH imaging of mouse kidneys in vivo using a frequency-dependent paraCEST agent. Magn Reson Med 2016;75(6):2432-2441.

21. Longo DL, Sun PZ, Consolino L, Michelotti FC, Uggeri F, Aime S. A general MRI-CEST ratiometric approach for pH imaging: demonstration of in vivo pH mapping with iobitridol. J Am Chem Soc 2014;136(41):14333-14336.

22. Muller-Lutz A, Khalil N, Schmitt B, Jellus V, Pentang G, Oeltzschner G, Antoch G, Lanzman RS, Wittsack HJ. Pilot study of Iopamidol-based quantitative pH imaging on a clinical 3T MR scanner. Magma 2014;27(6):477-485.

23. Stancanello J, Terreno E, Castelli DD, Cabella C, Uggeri F, Aime S. Development and validation of a smoothing-splines-based correction method for improving the analysis of CEST-MR images. Contrast Media Mol Imaging 2008;3(4):136-149.

24. Kim M, Gillen J, Landman BA, Zhou J, van Zijl PCM. Water saturation shift referencing (WASSR) for chemical exchange saturation transfer (CEST) experiments. Magn Reson Med 2009;61(6):1441-1450.

25. Cai K, Singh A, Poptani H, Li W, Yang S, Lu Y, Hariharan H, Zhou XJ, Reddy R. CEST signal at 2ppm (CEST@2ppm) from Z-spectral fitting correlates with creatine distribution in brain tumor. NMR Biomed 2015;28(1):1-8.

26. Sun PZ, Longo DL, Hu W, Xiao G, Wu R. Quantification of iopamidol multi-site chemical exchange properties for ratiometric chemical exchange saturation transfer (CEST) imaging of pH. Phys Med Biol 2014;59(16):4493.

27. Zhou IY, Wang E, Cheung JS, Zhang X, Fulci G, Sun PZ. Quantitative chemical exchange saturation transfer (CEST) MRI of glioma using Image Downsampling Expedited Adaptive Least-squares (IDEAL) fitting. Scientific Reports 2017;7(1):84.

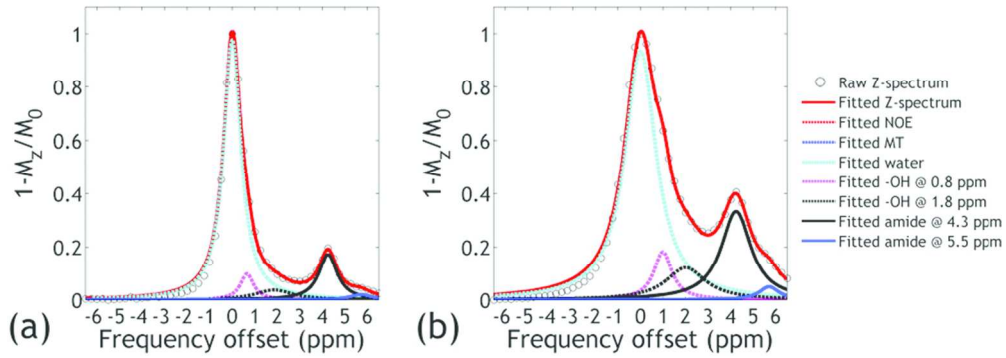

Figure 1. Multi-pool Lorentzian decoupling of representative CEST Z-spectra from pH vial of 7.0, obtained under B1 of (a) 1.0 μT and (b) 2.0 μT.

85x31mm (300 x 300 DPI)

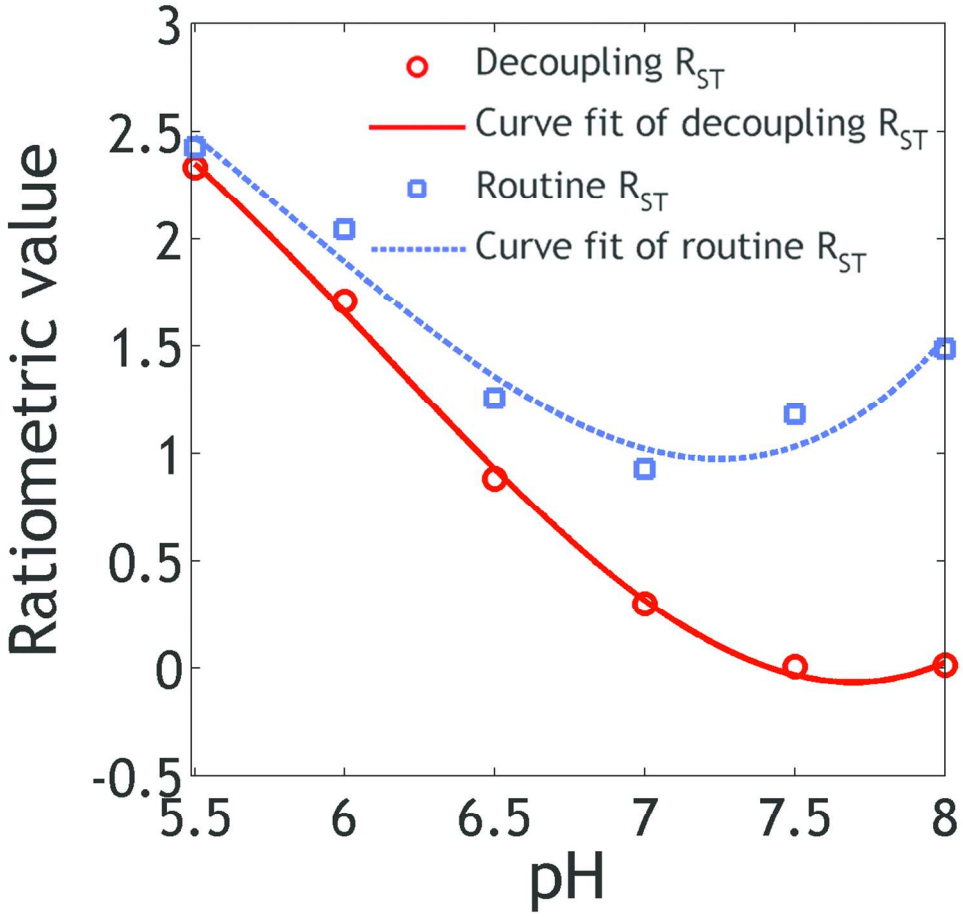

Figure 2. Extension of pH detection range using the modified ratiometric analysis (red circles) vs. that using the conventional simplistic ratiometric approach (blue squares).

115x106mm (300 x 300 DPI)

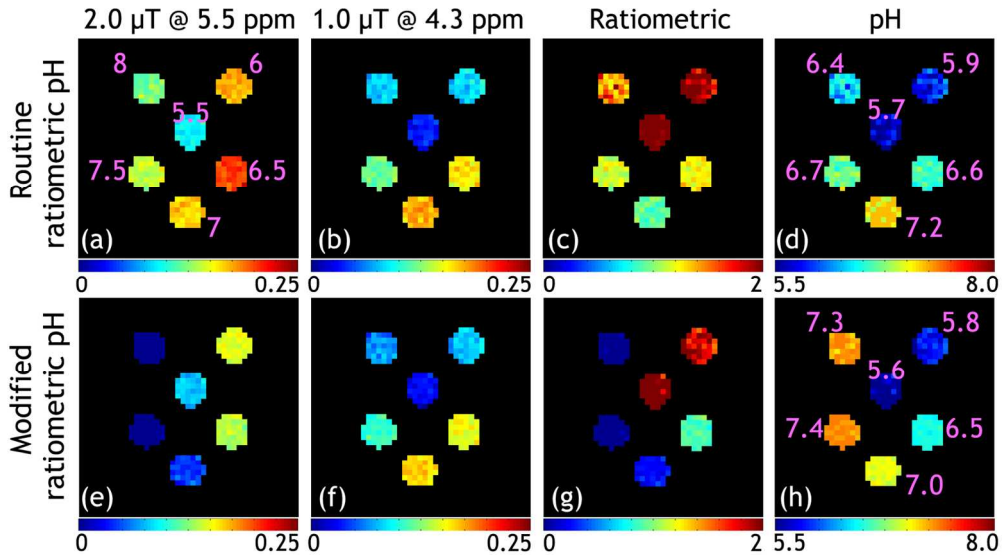

Figure 3. Simplistic CESTR images (a) at 5.5 ppm acquired at 2.0 μT and (b) at 4.3 ppm obtained under 1.0 μT. (c) Ratiometric images show good pH sensitivity until pH of 7.0 (d). In comparison, (e) and (f) show CEST images obtained from the line-decoupling, with the modified ratiometric image shown in (g) that can capture pH as high as 7.5 (h).

150x82mm (300 x 300 DPI)

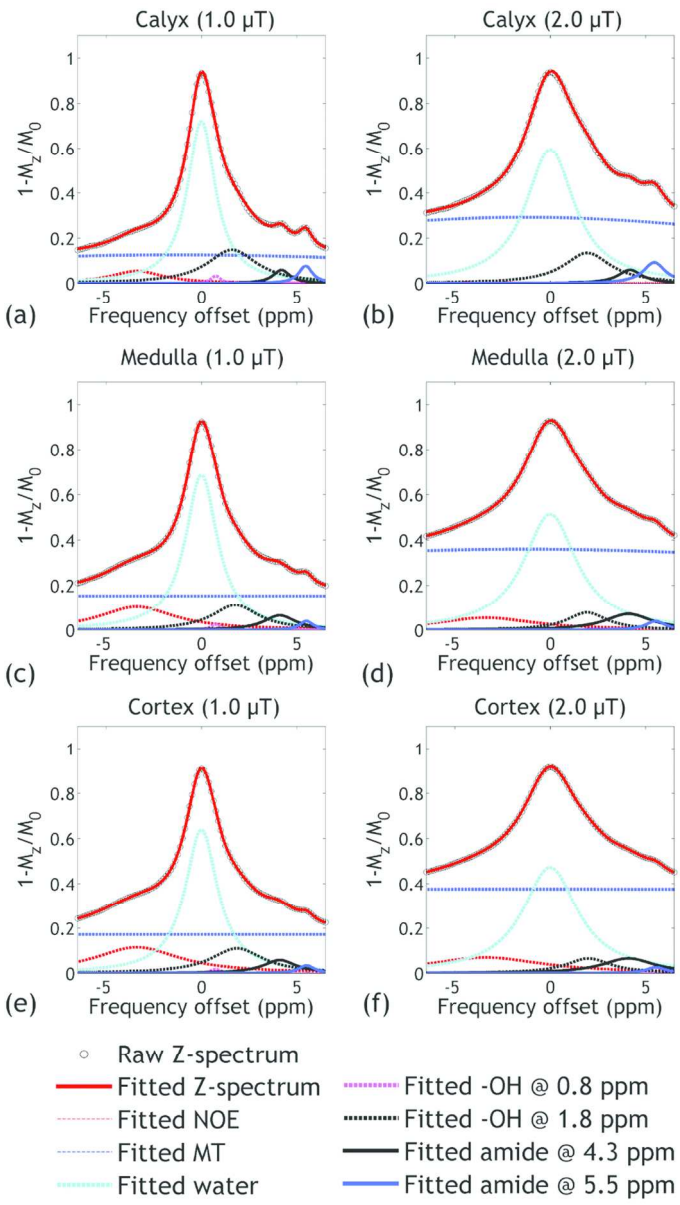

Figure 4. Inverted Z-spectra measured at calyx (a, b), medulla (c, d), and cortex (e, f) from B1 of 1.0 μT (left column) and 2.0 μT (right column) were fitted using a multi-pool Lorentzian model. ST effects at 5.5 ppm (B1=2.0 μT, right column) decreases substantially from calyx (b), medulla (d), to cortex (f), while ST effect at 4.3 ppm (B1=1.0 μT, left column) shows relatively small change (a, c, e).

85x151mm (300 x 300 DPI)

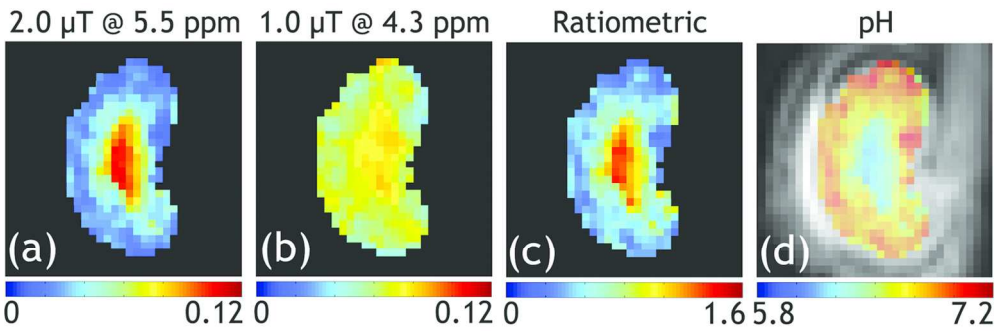

Figure 5. Demonstration of renal pH map from a representative rat. The resolved maps of ST effects at (a) 5.5 and (b) 4.3 ppm were obtained with the decoupling method, from which (c) the modified ratiometric map was obtained. (d) pH map overlaid on corresponding T2-weighted image shows renal pH gradually decreases from the cortex, medulla to calyx.

150x49mm (300 x 300 DPI)

SUPPLEMENTARY INFORMATION

A Generalized Ratiometric Chemical Exchange Saturation Transfer (CEST) MRI Approach for Mapping Renal pH using Iopamidol

Yin Wu, Iris Y. Zhou, Takahiro Igarashi, Dario L. Longo, Silvio Aime, and Phillip Zhe Sun

Data analysis

For the conventional non-decoupling methods, the ST effects at chemical shifts of 4.3 and 5.5 ppm were measured with asymmetric analysis of $ST(\omega) = \frac{M(-\omega) - M(\omega)}{M_0}$ where, ω is the chemical shift of iopamidol amide proton with respective water resonance, M_0 is signal intensity without RF irradiation. For the proposed decoupling methods, the ST effects at chemical shifts of 4.3 and 5.5 ppm were obtained by decoupling multi-pool CEST effects. Renal pH from ratiometric analysis of the same RF power level (e.g. ST(5.5 ppm)/ST(4.3 ppm) under 1.0 and 2.0 μT) and mixed RF power levels (e.g. ST(5.5 ppm, 2.0 μT)/ST(4.3 ppm, 1.0 μT)) was investigated for both of the proposed and conventional ratiometric analysis methods, respectively.

FIGURE CAPTIONS

Figure S1. ST effects at (a) 5.5 ppm and (b) 4.3 ppm under the same saturation power of 1.0 μT were measured with the conventional non-decoupling method, from which (c) the ratiometric map was obtained. (d) pH map overlaid on a T2-weighted image shows that pH values of most of voxels in inner layers were less than 5.8, deviating from reported values.

Figure S2. ST effects at (a) 5.5 ppm and (b) 4.3 ppm under the same saturation power of 2.0 μT were measured with the conventional non-decoupling method, from which (c) the ratiometric map was obtained. (d) pH map overlaid on a T2-weighted image shows that the renal pH values are apparently underestimated compared to reported values.

Figure S3. ST effects at (a) 5.5 ppm (B_1=2.0 μT) and (b) 4.3 ppm (B_1=1.0 μT) were measured with the conventional non-decoupling method, from which (c) the ratiometric map was obtained. (d) pH map overlaid on a T2-weighted image shows that renal pH values at middle layers (<5.8) are smaller than those at calyx, inconsistent with reported values and renal pH pattern.

Table S1. Renal pH values measured by ratioing CEST effects at different chemical shifts of 5.5 and 4.3 ppm obtained under saturation powers of 1.0 and 2.0 μT with the conventional non-decoupling and proposed decoupling methods. Mean ± standard deviation are presented.

		Cortex	Medulla	Calyx	Entire kidney
Non-decoupling method	1.0 μT	6.41±0.23	6.21±0.34	5.83±0.31	6.27±0.22
	2.0 μT	6.54±0.14	6.56±0.20	6.36±0.14	6.52±0.16
	2.0 μT/1.0 μT	6.32±0.31	6.05±0.22	5.93±0.20	6.19±0.23
Decoupling method	1.0 μT	6.31±0.23	6.28±0.14	5.95±0.28	6.26±0.21
	2.0 μT	6.66±0.17	6.61±0.11	6.44±0.16	6.61±0.14
	2.0 μT/1.0 μT	7.00±0.08	6.81±0.08	6.48±0.19	6.85±0.11

Figure S1.

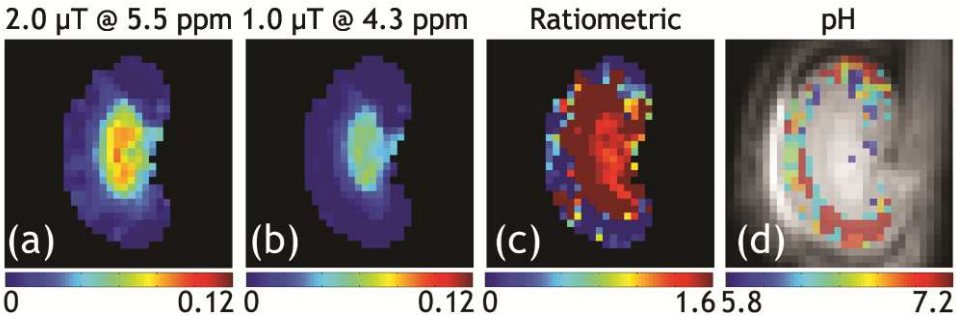

Figure S2.

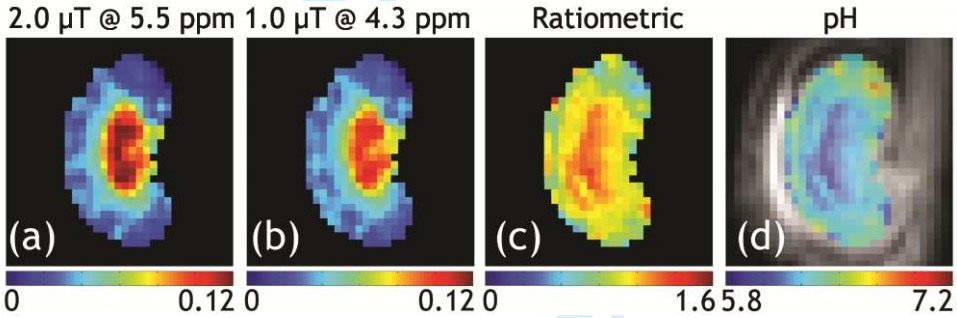

Figure S3.